A Lagrangian study of surface pCO_2 dynamics in the eastern equatorial Pacific Ocean

Michael D. DeGrandpre,[1] Rik Wanninkhof,[2] Wade R. McGillis,[3] and Peter G. Strutton[4]

Received 8 August 2003; revised 4 May 2004; accepted 3 June 2004; published 18 August 2004.

[1] We characterized pCO_2 variability on hourly to weekly timescales during the 14-day GasEx-2001 Lagrangian drifter experiment in the eastern equatorial Pacific Ocean. Underway pCO_2 was recorded at 5 m depth as the ship closely followed a drogued drifter. Dissolved O_2 (DO) was measured at 10 and 15 m depths using in situ sensors deployed on the drogue. Diel pCO_2 and DO variability is evaluated using a simple model that accounts for air-sea exchange, vertical mixing, heating, and net community metabolism. Mixed-layer depths and local (vertical) entrainment are estimated with the Price Weller Pinkel (PWP) mixed-layer model. The mean observed pCO_2 was 472.0 ± 1.8 μatm with a diel increase of 2–6 μatm on most days, near coincident in time with the diel peak in temperature. The biogeochemical model reveals that heating was the primary source of diel pCO_2 variability, but net community production and depletion of CO_2 in the shallow warm layer due to air-sea gas exchange reduced the heating-driven peak by ~1–4 and 1–2 μatm each day, respectively. The same model parameterizations also accurately predict the diel DO amplitude. In the model, atmospheric exchange depletes total CO_2 and DO in the surface layer, and the depleted water is mixed with the isolated underlying water during nocturnal convection. The 10- and 15-m DO time series corroborate these predicted dynamics. Over the 14-day study, net heating offset the expected ~14 μatm decrease due to air-sea CO_2 exchange and net community production, resulting in a nearly constant mean pCO_2. Consequently, net heating acts to sustain high air-sea CO_2 fluxes in the upwelled equatorial Pacific water as the water advects westward in the South Equatorial Current. *INDEX TERMS:* 4806 Oceanography: Biological and Chemical: Carbon cycling; 4805 Oceanography: Biological and Chemical: Biogeochemical cycles (1615); *KEYWORDS:* sea surface CO_2, biogeochemical dynamics, diurnal cycling

Citation: DeGrandpre, M. D., R. Wanninkhof, W. R. McGillis, and P. G. Strutton (2004), A Lagrangian study of surface pCO_2 dynamics in the eastern equatorial Pacific Ocean, *J. Geophys. Res.*, *109*, C08S07, doi:10.1029/2003JC002089.

1. Introduction

[2] Upwelling and nutrient limitation create high CO_2 supersaturation throughout the eastern equatorial Pacific Ocean. The equatorial Pacific sea to air CO_2 flux is 0.8–1.0 Pg C yr^{-1} during non–El Niño periods [*Feely et al.*, 2002]. The equatorial Pacific has been the focus of many oceanographic studies because of its importance in the global carbon cycle. Thanks to these studies, we now have a general picture of the inorganic carbon system (pCO_2, pH, DIC or total alkalinity) distributions in the equatorial Pacific [e.g., *Inoue and Sugimura*, 1992; *Murray et al.*, 1994; *Lefèvre et al.*, 1994; *Dandonneau*, 1995; *Wanninkhof et al.*, 1995; *Chavez et al.*, 1999; *Feely et al.*, 2002]. During non–El Niño periods, sea surface pCO_2 is typically 450–500 μatm in the eastern upwelling region, or >100 μatm above atmospheric equilibrium. Surface pCO_2 progressively decreases westward, and is near atmospheric levels in the western equatorial Pacific warm pool. Sea surface pCO_2 drops from east to west primarily through biological uptake and air-sea exchange of inorganic carbon [e.g., *Murray et al.*, 1994]. The contributions of these two processes have been determined using mass balances between different locations, assuming water advected from east to west locations [*Lefèvre et al.*, 1994; *Wanninkhof et al.*, 1995]. Accurately quantifying each process remains challenging, however, because estimates based on mapped distributions require many assumptions to derive rates of production and air-sea exchange.

[3] Other studies, particularly the recent equatorial Fe fertilization experiments, have tracked short-term CO_2 variability in a single water mass [*Watson et al.*, 1994; *Cooper et al.*, 1996; *Steinberg et al.*, 1998]. In the Fe studies, research vessels typically spend much of the time mapping

[1]Department of Chemistry, University of Montana, Missoula, Montana, USA.
[2]Atlantic Oceanographic and Meteorological Laboratory, National Oceanic and Atmospheric Administration, Miami, Florida, USA.
[3]Geochemistry, Lamont-Doherty Earth Observatory, Columbia University, Palisades, New York, USA.
[4]College of Oceanic and Atmospheric Sciences, Oregon State University, Corvallis, Oregon, USA.

0148-0227/04/2003JC002089$09.00

the surrounding region and a limited time in the water mass of interest. In fact, few continuous Lagrangian inorganic carbon data sets have been collected in the equatorial Pacific. Continuous Lagrangian data are more amenable to model interpretation and may therefore provide better quantitative estimates of the biogeochemical and physical processes that control pCO_2. With this knowledge, we can improve model parameterizations for predicting pCO_2 variability [e.g., *Chai et al.*, 2002] and further refine empirical pCO_2 relationships currently used to map pCO_2 distributions from satellite and mooring data [e.g., *Boutin et al.*, 1999; *Cosca et al.*, 2003]. Achievement of these goals will not only improve past, present, and future air-sea CO_2 flux estimates, but will also add to our fundamental understanding of biogeochemical cycles in aquatic ecosystems.

[4] In the present paper, we evaluate the processes that control short-term (hours to weeks) pCO_2 variability and assess the influence of these processes on the air-sea CO_2 flux in the upwelled water that is advected westward in the South Equatorial Current (SEC). We utilize a 14-day pCO_2 and dissolved O_2 (DO) Lagrangian time series collected in February–March 2001 during the NOAA GasEx-2001 experiment. The dissolved gas variability is interpreted with physical and biogeochemical mixed-layer models supported by ancillary shipboard and in situ measurements.

2. Study Site, Methods, and Model

[5] The hydrographic and physical settings for the experiment are described elsewhere [*Johnson et al.*, 2004; *Sabine et al.*, 2004]. In brief, a drogued drifter was deployed in the SEC on 15 February 2001. NOAA R/V *Ronald H. Brown* closely followed the drifter for a ~14-day period ending 1 March 2001. The drifter traveled ~715 km in a northwesterly direction during this period (Figure 1). Continuous underway pCO_2 measurements were made using an equilibrator-infrared system located in the ship's laboratory [*Wanninkhof and Thoning*, 1993; *Feely et al.*, 1998]. Flowing seawater was obtained from the seawater intake located at ~5 m depth on the ship's bow. Seawater and atmospheric pCO_2 were calculated from local barometric pressure (P), water vapor pressure at sea surface temperature (V_p) and the dried mole fraction of CO_2 (X_{CO2}) measured by the underway pCO_2 system according to $pCO_2 = (P - V_p)\, X_{CO2}$. Total dissolved inorganic carbon (DIC) measurements were made on hydrocast samples by acidifying a seawater aliquot and stripping all CO_2 from the water followed by a coulometric titration of the evolved CO_2 [*Johnson et al.*, 1985]. DO was measured using in situ amperometric sensors [*Langdon*, 1984] deployed on the drifter at 10 and 15 m. The DO sensors experienced a systematic drift during the study that was accounted for by normalizing the output to the Winkler DO determined from daily hydrocast profiles.

[6] A simple mixed layer physical-biogeochemical model is used to examine short-term pCO_2 and DO variability [*Baehr and DeGrandpre*, 2004]. Modeled pCO_2 is calculated from modeled DIC and alkalinity as described below. A two-box model is used to account for isolation of the warm surface layer during daytime heating. The boxes are bordered by the air-sea interface and the ~40-m-deep pycnocline present throughout the experiment [*Johnson et al.*, 2004]. The DIC and DO mass balances in the two boxes are expressed as

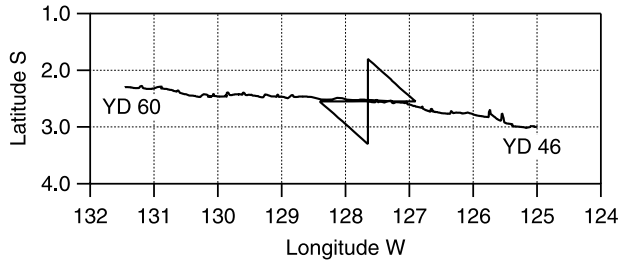

Figure 1. Cruise track of the NOAA R/V *Ronald H. Brown* during the 14-day Lagrangian experiment in February–March 2001 (YD 46–60). The drifter followed the path from 125°W to 131.5°W. A butterfly patterned survey was conducted from YD 52.8–54 to determine spatial gradients around the drifter as noted by the large excursion from the drifter track around 127.7°W. The small spikes were periods when the ship moved away from the drifter to pump waste.

$$H\frac{dC}{dt} = F_{GAS} + F_{NCM} + F_{ENT} + F_{ADV}, \quad (1)$$

where H is either the surface mixed layer depth (MLD) or the underlying layer above the deep pycnocline (i.e., 40 m – MLD), and $\frac{dC}{dt}$ is the rate of change of DIC or DO due to air-sea gas exchange (F_{GAS}), net community metabolism (F_{NCM}), vertical entrainment (F_{ENT}), and advection of different water masses (F_{ADV}). All model fluxes are calculated using a 0.5-hour time step. On the basis of current velocities, the drifter diverged slightly from the path of the original water mass [*Johnson et al.*, 2004], but because horizontal gradients were small, we assume horizontal advection was negligible. Vertical advection (upwelling) and eddy diffusion also did not significantly change the mass balance [*Sabine et al.*, 2004].

[7] Air-sea CO_2 flux (F_{GAS}) is estimated by

$$F_{GAS} = kS\Delta C, \quad (2)$$

where k is the gas transfer velocity, S is gas solubility, and ΔC is the CO_2 or DO partial pressure difference between the atmosphere and surface mixed layer. The gas transfer velocity is estimated using a variety of available parameterizations [*Liss and Merlivat*, 1986; *Wanninkhof*, 1992; *McGillis et al.*, 2004] and the wind speed at 10 m above the sea surface. The Schmidt number (Sc) equations of *Wanninkhof* [1992] are used to calculate k for different temperatures and gases (i.e., DO). The cool skin effect [*Van Scoy et al.*, 1995] is not included in the flux calculation because its short-term effect on the CO_2 flux is not significant [*Ward et al.*, 2004].

[8] F_{NCM} is the difference between gross primary production (P) and community respiration (R). The rate of community respiration is assumed to be constant (see section 4). Primary production is assumed to have a light and chlorophyll-a dependent behavior described by

$$P = \left[\mathrm{Chl}{-}a\left(P_s\mathrm{Chl}^{-1}\right)\left(1 - e^{-a}\right)e^{-b}\right], \quad (3)$$

where P is primary production in mg C m^{-3} h^{-1} (C = carbon), Chl-a is the concentration of chlorophyll-a

(mg m^{-3}), P_s Chl^{-1} is the assimilation number or Chl-*a* specific maximum rate of photosynthesis in the absence of photoinhibition (mg C mg Chl-a^{-1} h^{-1}), $a = [\alpha Q_{PAR}(P_s\ \text{Chl}^{-1})^{-1}]$, α is the Chl-*a* specific rate of light limited photosynthesis (mg C mg Chl-a^{-1} h^{-1} (μmol quanta m^{-2} s^{-1})$^{-1}$), Q_{PAR} is the downwelling photosynthetically available radiation (PAR, μmol quanta m^{-2} s^{-1}), $b = [\beta Q_{PAR}(P_s\ \text{Chl}^{-1})^{-1}]$ and β is the Chl-*a* specific photoinhibition parameter (mg C mg Chl-a^{-1} h^{-1} (μmol quanta m^{-2} s^{-1})$^{-1}$) [*Platt et al.*, 1980; *Cullen et al.*, 1992]. Q_{PAR} was estimated from daily irradiance profiles obtained with a Satlantic SeaWiFS Profiling Multispectral Radiometer (SPMR). Mean Q_{PAR} at 5 m and 25 m (the assumed mean depths for the upper and lower box) were 78% and 29% of the incident solar radiation at the surface, respectively. The DO model uses photosynthetic and respiratory quotients (PQ, RQ) of 1.4 and 1.0, respectively, as explained below. We discuss other specific parameter values in section 3. In the remaining text, F_{NCM} is represented as its more conventional form (NCM). When NCM is positive it is referred to as net community production (NCP).

[9] The depth range of the two boxes (H in equation (1)) and vertical entrainment (F_{ENT}) are estimated using the PWP mixed-layer model [*Price et al.*, 1986]. The model requires an initial temperature and salinity profile and time series of air-sea heat flux, wind, wind direction, precipitation, and evaporation (Figure 2). The MLD is defined as water homogeneous to within 0.001 kg m^{-3} over the depth interval of the model (0.01 m). The model simulates variability at 5 m by using the 5-m temperature, PAR and Chl-*a* averaged between 2 and 10 m, but the surface box still undergoes air-sea exchange even if the MLD is <5 m. Therefore, the 5-m modeled record reflects the variability of a layer always in contact with the atmosphere. Deepening of the mixed layer entrains water from the deeper box and the new surface DIC or DO concentrations are estimated by mass balance. The model imposes that mixing does not impact bottom box concentrations until the MLD reaches 20 m, thereby simulating the dynamics of measurements at 20 m. If the surface layer extends below 20 m, bottom box concentrations are calculated from mass balance between 40 m and the entrainment depth. The MLD time series (below) suggest that vertical mixing was never sufficient to entrain the deep (~40 m) pycnocline water into the mixed layer.

[10] The modeled DIC and total alkalinity (TA) is used to compute pCO_2 at each time step. TA, derived from discrete pCO_2 and DIC measurements on hydrocast samples, was nearly constant during the 14-day study with a mean value of 2323.4 ± 1.2 μmol kg^{-1}. The CO_2 equilibrium constants are calculated from *Dickson and Millero* [1987] and CO_2 solubility from *Weiss* [1974] using the temperature and salinity measured at the seawater intake (5 m depth). The initial calculated pCO_2 was ~11 μatm lower than the shipboard pCO_2, apparently due to an error in the calculated TA. Therefore 11 μatm is added to the modeled pCO_2 to correct for this offset.

3. Results

3.1. Overview

[11] The data input into the physical model are shown in Figure 2 along with the MLD predicted with the PWP model. The meteorological forcings were characterized by winds averaging 6.0 ± 1.3 m s^{-1}, partly overcast skies, and a major rain event with ~3 cm accumulation. A shallow warm layer formed each day as shown by the modeled MLD (Figure 2). Nocturnal convection eroded the warm layer, and the surface mixed layer reached a maximum depth in the early morning ranging from 5 to 33 m. On YD 51, low winds, combined with reduced surface salinity due to the rain event, impeded convective mixing and the MLD remained <6 m for over 24 hours (Figures 2 and 3). Daily net heat input also increased surface temperature by ~0.7°C over the 14-day period (Figure 3).

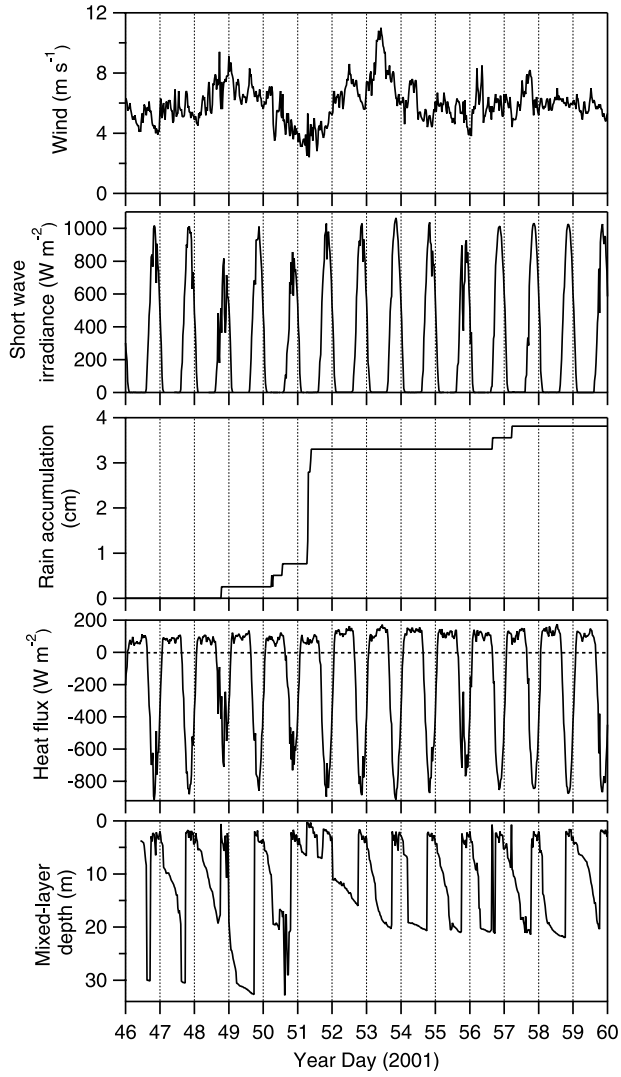

Figure 2. Meteorological data used for input into the PWP model [*Price et al.*, 1986] (top four panels) and the mixed-layer depth (MLD) output from the model (bottom panel). The MLD was used to model vertical entrainment in the two-box biogeochemical model. Year Day is UTC. 0000 UTC is 1600 local time.

[12] The pCO_2 was nearly constant during the 14-day period with a mean value of 472.0 ± 1.8 μatm, ~120 μatm above atmospheric equilibrium (Figure 3). A ~2–6 μatm diel peak was observed on most days. The diel pCO_2 reached a maximum between 2200 and 2400 UTC (1400 to 1600 local time), following the maximum in solar

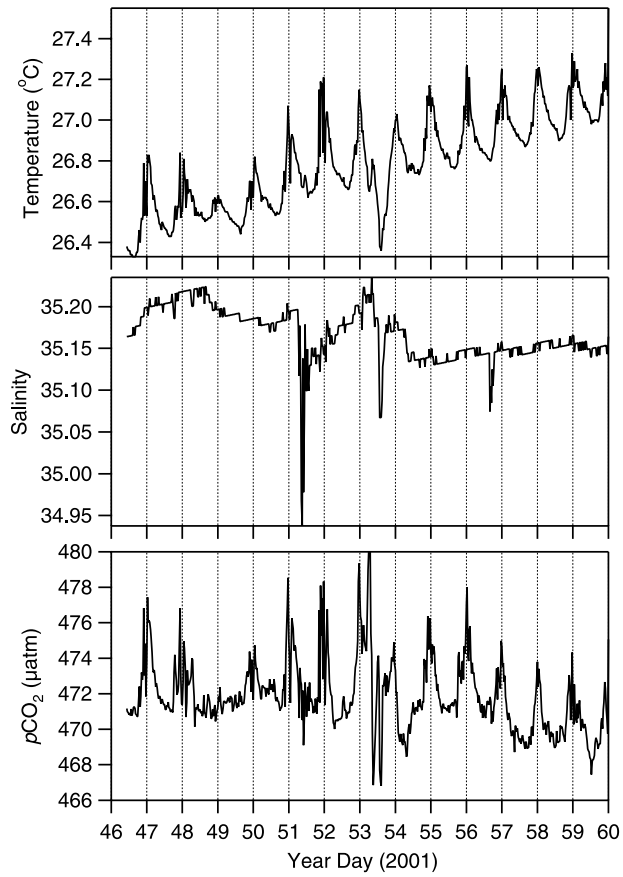

Figure 3. Shipboard time series from the seawater intake at 5 m depth. The temperature and salinity were measured close to the intake in the ship's bow. The pCO_2 was measured using an equilibrator-infrared system in the ship's laboratory. A sense of horizontal gradients is given by data during YD 52.8–54 when the ship's ~80-km butterfly pattern was undertaken (Figure 1).

insolation by 1.5–3.5 hours (2030 UTC, Figure 2), but typically leading the peak in temperature by ~1.5 hours. The slight phase difference between the pCO_2 and temperature maxima suggests that heating was not the only source of diel variability. A second more obvious feature is that the diel heating led to a diel increase in pCO_2, but the net ~0.7°C temperature increase appeared to have no effect on the ~471 µatm pCO_2 baseline (Figure 3). The ~14 µatm increase in pCO_2 expected from ~0.7°C net heating was apparently offset by other CO_2 sinks that operated on the same timescale as the daily net heat flux. These underlying mechanisms are examined using the model described above.

3.2. Model Results

[13] The effects of heating are examined by using a simplified single-box form of the model (referred to as M1). M1 assumes a constant 30-m MLD (F_{ENT} = 0), no biological contribution (NCM = 0), and air-sea exchange (F_{GAS}) parameterized using equations from *Wanninkhof* [1992] (referred to as W92). M1 predicts the observed variability remarkably well, with a mean error <2 µatm (Table 1, Figures 4a and 4b). The residual pCO_2 error reveals, however, that the model does not account for approximately 50% of the observed diel pCO_2 cycle (Figure 4b). The typical ~0.4°C diel heating cycle (Figure 3) should increase pCO_2 by ~8 µatm based on equilibrium calculations. The observed diel amplitudes are somewhat less than this (compare M1 and data in Figure 4a). Modeled pCO_2 is too high in the late afternoon (~0000 UTC) and too low in the early morning (Figure 4b), suggesting that another mechanism is contributing to the diel pCO_2 cycle. M1 is able to match the long-term trend in pCO_2 by predicting the observed DIC decrease

Table 1. Model Error for Different Model Forms[a]

Model Conditions	Mean Model Error, µatm
M1: 30-m MLD, no biology	1.7
M2: two-box model, no biology	2.3
M3: full model	1.6

[a]The mean of the absolute value of modeled-measured pCO_2.

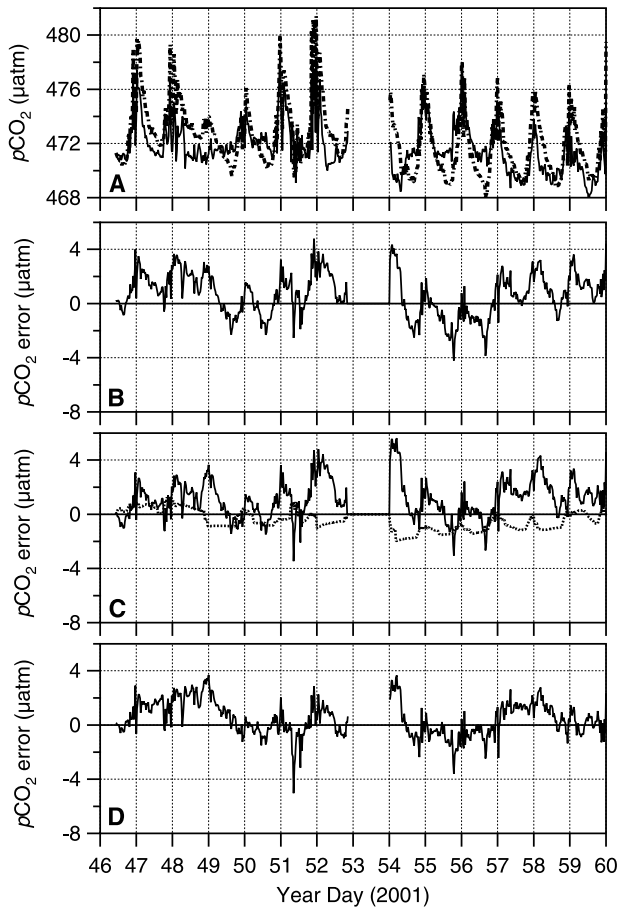

Figure 4. Error in µatm from different models (Table 1) calculated as modeled-measured pCO_2. (a) M1 pCO_2 prediction (dotted line) and measured pCO_2 (solid line). (b) Residual diel signal from M1 is attributed to diel CO_2 depletion in the shallow warm layer and net uptake of CO_2 by phytoplankton during the day. (c) M2, which uses a realistic MLD, accounts for the air-sea depletion in the warm layer as noted by the difference between M1 and M2 (dotted line). (d) Full model M3, which uses a simple chl-*a* and light-dependent model of primary production, accounts for most of the remaining diel variability. The data collected during the butterfly survey are omitted (YD 52.8–54) (Note that 0000 UTC is 1600 local time).

in the mixed layer over the 14-day period. Shipboard measurements found that DIC dropped from ~2038 to 2031 μmol kg^{-1} during the course of the study (Figure 5). We use a 30-m MLD in M1 because this MLD gives the ~7 μmol kg^{-1} loss of DIC (due only to air-sea exchange in this simplified model). M1 therefore confirms that the observed DIC loss negated the increase in pCO_2 expected by warming; that is, increasing temperature by ~0.7°C and decreasing DIC by ~7 μmol kg^{-1} with constant alkalinity results in a nearly constant pCO_2. On diel timescales, the mechanisms for DIC loss damp but do not eliminate the heating driven signal. The two-box model described above is used in order to explore these additional sources of diel variability and long-term DIC loss.

[14] NCM is again set equal to zero to focus on the role of mixing and air-sea exchange (using W92) in the diel pCO_2 signal. The mean error for this model is 2.3 μatm (M2, Table 1). A residual diel pCO_2 error is still present although it is reduced relative to M1 (Figure 4c). The modeled DIC reveals that air-sea exchange can deplete DIC in the isolated surface layer (Figure 5a). During the day, DIC is 0.5–1 μmol kg^{-1} lower than DIC below the mixed layer. The maximum depletion occurs during an extended period of shallow MLDs (YD 51–53, Figures 2 and 5a). During most diel periods, nocturnal convection mixes the DIC-depleted surface water with subsurface water and the DIC in the two layers converge (Figure 5a). These diel changes in DIC result in a small diel change in pCO_2 as shown by the difference between models with and without mixed-layer dynamics (M1–M2, Figure 4c). M2 predicts lower pCO_2 than M1 in the late afternoon; that is, the depletion acts in the opposite direction of the heat-driven pCO_2. Over a diel cycle, the depletion and nocturnal mixing account for ~1–2 μatm of the observed diel amplitude (Figure 4c). M2 also accounts for most of the DIC loss during the 14-day period (Figure 5a), implying that all but ~1.0–1.5 μmol kg^{-1} of the DIC is lost through air-sea exchange (when using the W92 gas transfer rates). The sensitivity to different gas transfer parameterizations is discussed below.

[15] Biological uptake of CO_2 is the most likely mechanism accounting for the remaining 1–4 μatm diel pCO_2 variability not explained by M2 (Figure 4c). We examine the photosynthetic contribution using the primary production model described in equation (3). The model parameters for equation (3) have been quantified by *Cullen et al.* [1992] along 150°W in the equatorial Pacific. The rates of production using their assimilation numbers (P_s Chl^{-1}) were never sufficient to reproduce the estimated diel change in pCO_2. A P_s Chl^{-1} of 10 mg C (mg Chl-*a*)$^{-1}$ hr^{-1}, ~1.5–2 times greater than those reported by *Cullen et al.* [1992], is needed to generate a 1–4 μatm diel signal and the ~1.5–2.0 μmol kg^{-1} change in DIC observed during 24-hour intensive shipboard measurements (Figure 5). The P_s Chl^{-1} from *Cullen et al.* [1992] were derived from ^{14}C measurements. ^{14}C rates of primary production typically fall between net and gross production. Because we model respiration as a separate term, P in equation (3) estimates gross production [e.g., see *Bidigare et al.*, 1992] and is consequently larger than P used to describe ^{14}C production. The chl-specific rate of light limited photosynthesis (α) is adjusted so that (Ps Chl^{-1})α^{-1} (I_k in the work of *Cullen et al.* [1992]) is equal to 350 and 250 μmol quanta m^{-2} s^{-1} in the top and bottom layers (α = 0.029 and 0.040 mg C mg Chl-*a*$^{-1}$ h^{-1} (μmol quanta m^{-2} s^{-1})$^{-1}$), respectively. Since the light level at which saturation occurs is a fundamental physiological parameter of autotrophs [*Platt and Jassby*, 1976], we chose to constrain I_k in the model development. The photoinhibition parameter (β) is set equal to zero (equation (3)). Photoinhibition is known to occur in equatorial surface waters [*Cullen et al.*, 1992; *Strutton et al.*, 2004]; however, the dynamic range and vertical resolution of the data are not sufficient to critically examine the relatively weak influence of this parameter. A respiration rate of 1.32 μmol C kg^{-1} d^{-1} is used because it reproduces the observed diel DIC amplitude and balances the net uptake of CO_2 by the photosynthetic biomass over the 14-day period. In other words, NCM(= $P - R$) is constrained by the difference between the ~7 μmol kg^{-1} DIC decrease (Figure 5) and amount of DIC lost to air-sea exchange. The resulting R is comparable to respiration rates determined by the dark O_2 consumption method for other open ocean regions [e.g., *Williams*, 1998]. The full model (M3), using the W92 gas exchange rate, has a mean pCO_2 error of 1.6 μatm (Table 1). The residual diel pCO_2 error is reduced when NCM is included in the two-box model (Figure 4d).

[16] M3 can be used to examine DO variability by converting NCM from mols carbon to mols O_2 using the photosynthetic and respiratory quotients (PQ, RQ). Unlike

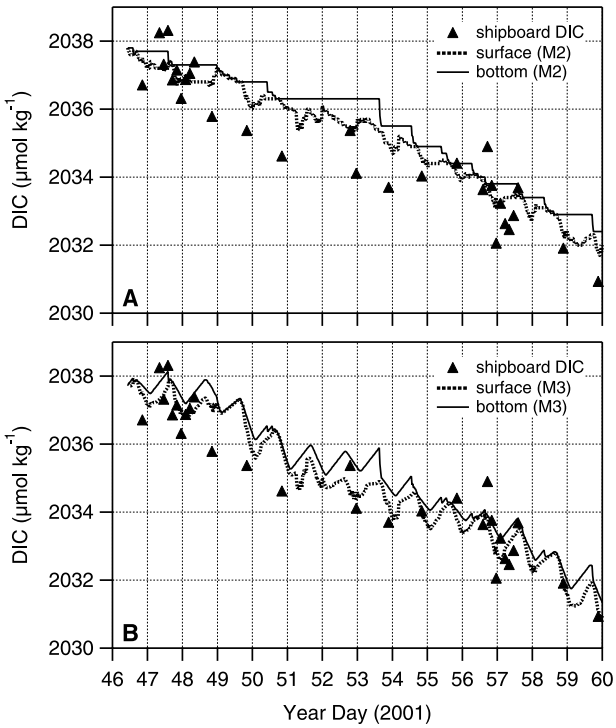

Figure 5. Modeled DIC in the surface and bottom boxes for models (a) M2 and (b) M3. Concentrations often converged around 1200 UTC (0400 local time) due to nocturnal convection and diverged during the day when the warm layer formed (see MLD in Figure 2). The shipboard DIC averaged over 0–30 m are also shown on both plots (solid triangles). Two intensive measurement periods (YD 47–48 and 56–57) revealed that DIC varied by 1.5–2.0 μmol kg^{-1} over a diel cycle.

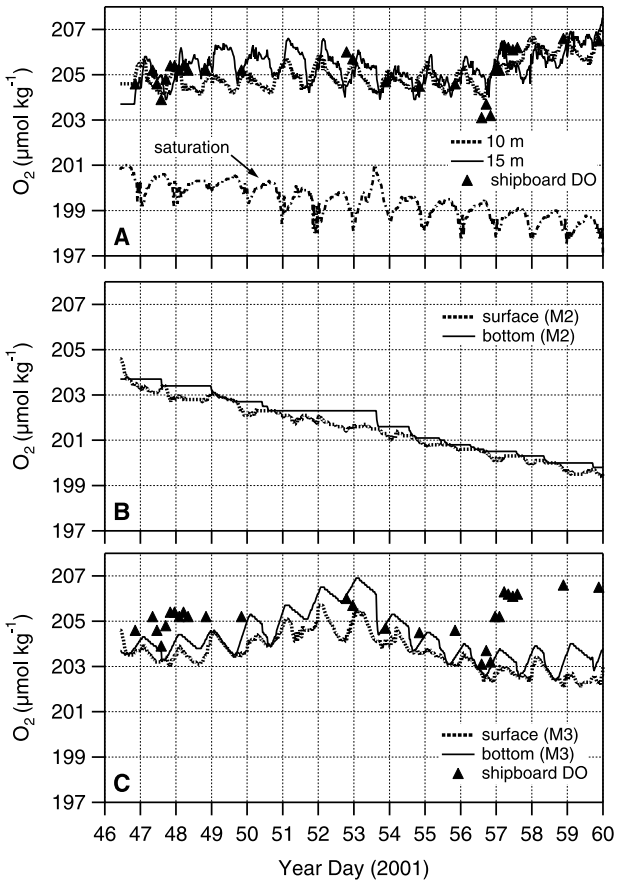

Figure 6. Dissolved O_2 (a) measured at two depths and (b, c) modeled in the surface and bottom boxes. The DO predictions use the same parameters for NCM as the CO_2 model, converting mols of carbon with PQ and RQ of 1.4 and 1.0, respectively. Atmospheric saturation (dotted line in Figure 6a) and shipboard DO in Figures 6a and 6c (solid triangles) are also shown.

pCO_2, heating does not directly change DO, and consequently, diel variability should primarily originate from NCM, air-sea gas exchange, and diel mixing. Second, net production of O_2 acts in the opposite direction of air-sea exchange because DO was supersaturated during the study (Figure 6a). Using M3 with the NCM parameters discussed above, the model predicts the observed amplitude of the DO diel signal (Figure 6c), supporting the model descriptions of NCM and mixing. The depth-resolved DO records and model also reveal information about the warm layer dynamics and their potential impact on pCO_2. Like pCO_2, DO supersaturation leads to depletion in the diel warm layer (M2, Figure 6b). The two DO records at 10 and 15 m show that DO was often lower closer to the surface and that concentrations became more uniform in the early morning. The two-box DO model reproduces much of the short-term variability between the two depths (Figures 6a and 6c). For example, DO often abruptly dropped around daybreak in the 15-m record. The model predicts similar variability and reveals that the sudden decrease is primarily due to entrainment of lower DO surface water down to the depth of the sensor (see MLD in Figure 2). In M3, losses to the atmosphere and lower net production both contribute to lower daytime DO levels at the surface relative to the underlying water. In an analysis of their depth-resolved DO records, *McNeil and Farmer* [1995] found that convective mixing modified the phase and amplitude of the diel DO signal. As pointed out in their work, single depth measurements of DO (or DIC) should not be used to estimate rates of primary production during periods of convective mixing.

[17] Unlike the pCO_2 model, M3 does not accurately reproduce the long-term DO variability (Figure 6). Because Chl-*a* is lower in the latter half of the time series (Figure 7), the modeled DO drops as net production no longer keeps pace with gas evasion. The observed DO increases during this time, however (Figure 6a). The DO model also requires PQ and RQ of 1.4 and 1.0 [*Laws*, 1991], respectively, to sustain a 4–5 μmol kg^{-1} DO supersaturation. Without the increased molar production of DO relative to DIC consumption, gas evasion draws DO down even more significantly. M2 in Figure 6b represents an extreme example where NCM = 0. The pCO_2 also decreased more significantly after YD 57 (Figure 3), which suggests, along with the DO and

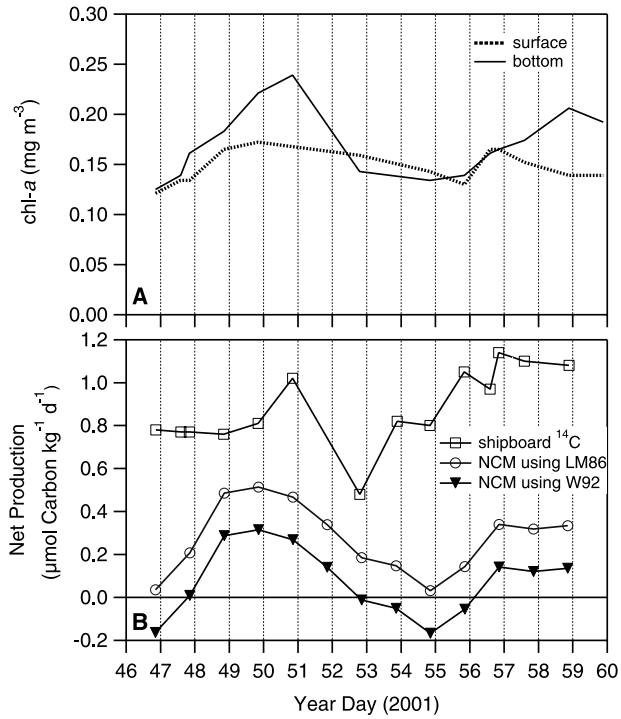

Figure 7. (a) Interpolated chl-*a* time series used in equation (3). Data were obtained from daily hydrocast samples. The surface and bottom records are the average chl-*a* concentrations between 2–10 m and 20–30 m, respectively. (b) Rates of primary production measured by ^{14}C on hydrocast samples averaged over 0–30 m depth and modeled rates of net community metabolism (NCM) using different air-sea gas exchange rates (LM86, W92). ^{14}C rates were 24-hour incubations onboard ship with light levels consistent with the sample depths. Mean (24 hour) NCM was calculated using equation (3) and a constant rate of respiration (W92: R = 1.32 μmol C kg^{-1} d^{-1}; LM86: R = 1.12 μmol C kg^{-1} d^{-1}).

^{14}C production time series (Figure 7b), that an unknown process increased primary production during this time. It is also clear that other forcings were altering the planktonic community. The 20–30 m average Chl-*a* doubled in the first 4 days, then rapidly declined and rose again (Figure 7a). The changes in Chl-*a* and primary production have no definitive connection to any physical forcing, although it was somewhat more cloudy and rainy from YD 49 to 51 and nocturnal convection was reduced (Figure 2, YD 51–52) when they had their sharpest decline. These changes may be related to decreased phytoplankton growth under reduced insolation (Figure 2) and, more speculatively, increased production after YD 52 due to wet deposition of Fe. *Gao et al.* [2003] have estimated that wet deposition is the primary source of aeolian dust to open ocean surface waters. Fe scavenged during the downpour on YD 51 would have slowly penetrated into subsurface waters as the MLD deepened from ~5 to 20 m over the period YD 51–53 (Figure 2), perhaps explaining the slow increase in Chl-*a* and primary production during this time (Figure 7). The assimilation number in equation (3) is dependent upon many different forcings, including atmospheric Fe input [*Barber and Chavez*, 1991], but we did not have sufficient information to explicitly model other processes. Alternatively, *Strutton et al.* [2004] suggest that shoaling of the deep pycnocline, which brings limiting nutrients higher up into the euphotic zone, contributed to the increase in primary production later in the study (Figure 7b). Although closure of the heat budget by *Johnson et al.* [2004] suggests that upwelling was minimal, it cannot be completely ruled out and could also account for the change in primary production.

4. Discussion and Conclusions

[18] The diel pCO_2 variability observed during the Lagrangian experiment was dominated by three mechanisms listed in order of significance: heating, NCM, and depletion in the warm surface layer. Diel surface heating of ~0.4°C drove an ~8 μatm increase in pCO_2 that was damped by NCM (1–4 μatm) and DIC depletion in the warm layer (1–2 μatm). These combined processes resulted in a 1–7 μatm diel increase in pCO_2, or a change in the mean ΔpCO_2 (118 μatm) of 0.8–5.9%. The diel variability therefore has a relatively small effect on the air-sea flux compared to present-day uncertainties that result from poor spatial and seasonal pCO_2 coverage (~±20%) [*Takahashi et al.*, 2002]. The diel pCO_2 cycle has also been shown to be dominated by diel heating in other open ocean regions, for example, summer in the North Atlantic (BATS) [*Bates et al.*, 1998]. In coastal waters, however, NCM typically overcomes heating and pCO_2 drops during daylight hours [e.g., *DeGrandpre et al.*, 1998].

[19] The pCO_2 was surprisingly constant over the 14-day period, particularly in contrast to mixed-layer temperature, which increased by ~0.7°C (Figure 2), and Chl-*a*, which varied by a factor of 2 (Figure 7a). As discussed above, the loss of ~7 μmol kg^{-1} DIC at constant alkalinity compensated for the pCO_2 increase due to net heating. Heating and DIC loss mechanisms are obviously very important in determining sea surface pCO_2 and the pCO_2 relationship to SST. Compelling evidence is presented by *Johnson et al.* [2004] that upwelling and other water mass inputs were minimal; therefore loss of CO_2 to the atmosphere and net community production must account for the drop in DIC. If air-sea exchange is estimated with available gas transfer models, the remaining loss of DIC can be attributed to net production. However, because of uncertainty in the gas transfer velocity, air-sea exchange does not adequately constrain net production. As presented above, if the W92 gas transfer parameterization is used, 5.5–6.0 μmol kg^{-1} of the 7.0 μmol kg^{-1} is due to gas evasion (M2, Figure 5b). The Liss-Merlivat (LM86) equations [*Liss and Merlivat*, 1986] and a relationship for the equatorial Pacific found by *McGillis et al.* [2004] have average k ~54% and 17% lower (equation (2)), respectively, than the W92 parameterization. The LM86 parameterization predicts a ~3 μmol kg^{-1} loss of DIC to the atmosphere. Net community production must take up the remaining ~4 μmol kg^{-1}. The mean daily DIC biological drawdown therefore ranges from 0.10 (W92) to 0.29 (LM86) μmol C kg^{-1} d^{-1} or 17–66% of the total DIC loss (Figures 5 and 7b). However, the higher rate of gas exchange given by the W92 equations results in a rate closer to the f-ratio-based estimates of new production (0.15 μmol C kg^{-1} d^{-1}) [*Strutton et al.*, 2004] and the observed NO_3 drawdown (0.16 μmol C kg^{-1} d^{-1}) assuming a 7:1 molar ratio between CO_2 and NO_3. Using the W92 gas exchange rate, over the 14-day period, pCO_2 drops by 12 μatm due to air-sea exchange (5.5 μmol kg^{-1} loss of DIC) and 3 μatm from net community production (~1.5 μmol kg^{-1} loss of DIC), but heating increases pCO_2 by ~14 μatm, resulting in a small net decrease in pCO_2 (Figure 3). Net heating therefore sustains high sea surface pCO_2 and consequently high air-sea CO_2 fluxes in the eastern equatorial Pacific.

[20] The resulting 24-hour mean NCM for the W92 and LM86 gas exchange models lie below the 24-hour ^{14}C volumetric primary production (Figure 7b) [*Strutton et al.*, 2004]. Many studies have shown that ^{14}C-based production estimates rates between net and gross primary production [e.g., *Langdon et al.*, 1995]. During an equatorial Pacific time series, *Walsh et al.* [1995] found that ^{14}C production was larger than net production derived from diel particle loading. If water mass changes are insignificant, diel mixed-layer inventories of particles, DO, or DIC are primarily controlled by community metabolism. These measurements therefore provide more direct insight into biological controls on surface pCO_2 variability than ^{14}C measurements.

[21] The present analysis suggests that pCO_2 and DIC variability in this section of the South Equatorial Current is dominated by local processes (for non–El Niño periods). Other studies have found that upwelling counterbalances DIC losses close to the equator but that biological uptake and gas exchange control the east-west gradient at 2°S, near the latitude of our study [*Wanninkhof et al.*, 1995]. Upwelling is also known to contribute more significantly during the equatorial cool season (July–December) [*Wanninkhof et al.*, 1995; *Cosca et al.*, 2003]. Our results suggest a weaker role of biological uptake in regulating equatorial Pacific sea surface pCO_2 than that estimated by *Lefèvre et al.* [1994]. Their rate of biological drawdown exceeds gas evasion by a factor of 7 for levels of CO_2 supersaturation similar to this study (~100 μatm) using the LM86 parameterization. However, gas evasion and biological uptake are nearly equal in their contribution when LM86 is used in our model. These differences in mass

balance estimates may be related to the choice of MLD used in the calculations. Because air-sea exchange scales as MLD^{-1} (equation (1)) and new production scales with MLD (MLD $\times$ $\Delta NO3/\Delta t$), unrealistically deep mixed-layers systematically underpredict and overpredict these processes, respectively. The *Lefèvre et al.* [1994] predictions were based on MLDs estimated from CTD casts at each station. It is unclear if constant or coarsely resolved (in time) MLDs are appropriate for such calculations. Using the mean of our high-resolution MLD time series (11.6 m, Figure 2) results in an unrealistically large loss due to air-sea exchange for both W92 and LM86. A 28-m MLD fits the data with the M3 parameterization, which is close to the mean maximum depth of the nocturnal MLD (24 m). Prediction of the local forcing effects on sea surface pCO_2 may require a high temporal resolution MLD rather than one determined by periodic hydrocasts or climatology.

[22] In this study, the 14-day Lagrangian pCO_2 time series did not correlate with temperature ($R^2 < 0.05$) because of the counterbalancing effects of heating, NCM, and air-sea gas exchange. Sea surface pCO_2-SST relationships have been extensively examined in the equatorial Pacific [e.g., *Boutin et al.*, 1999; *Chavez et al.*, 1999; *Cosca et al.*, 2003]. These relationships have been used to generate pCO_2 distributions in the equatorial Pacific for air-sea flux calculations [e.g., *Cosca et al.*, 2003]. Sea surface pCO_2 is typically negatively correlated with temperature, reflecting the dominance of upwelling in the region. The relationships have considerable scatter, however, even when split into seasonal and El Niño/non–El Niño time periods ($R^2 < 0.6$ typically [*Cosca et al.*, 2003]). Although the present study encompasses a small pCO_2 and temperature range, presumably heating, NCM, and air-sea exchange continue to damp pCO_2 variability as upwelled water moves west in the SEC. These effects result in a smaller negative slope between pCO_2 and SST and may explain the different relationships between warm and cool seasons [*Cosca et al.*, 2003]. If no upwelling or other mixing occurs in the SEC, the net heat flux will gradually decrease and temperature will reach a plateau. At this point, pCO_2 will begin to decline more rapidly as NCM and gas evasion dominate. The steeper pCO_2-SST relationship evident between 28° and 30°C may originate from these dynamic effects [*Boutin et al.*, 1999; *Cosca et al.*, 2003]. These observations may guide further improvement in pCO_2-SST relationships; for example, the air-sea temperature difference may be an important additional variable to consider.

[23] Continuous Lagrangian biogeochemical time series are rare, yet can provide a very powerful data set for model interpretation. The equatorial Pacific's SEC proved particularly amenable to Lagrangian study, and follow-up Lagrangian experiments should be directed at further constraining NCM and thereby providing a better estimate of air-sea gas exchange rates in the region. The pCO_2 and DO results support that we have a basic understanding of the processes that control pCO_2 in surface waters, yet many interesting and challenging questions remain; for example, quantitative connections between pCO_2, food web dynamics, and net community production must be established.

[24] **Acknowledgments.** We thank Robert Castle for tending the underway pCO_2 system and for post-cruise data analysis, Marilyn Lamb for DIC measurements, Charles Fisher for oxygen analyses, and Will Drennan and Jim Edson for the meteorological and heat flux data. The PWP code was generously provided by Jim Price. We also thank the captain and crew of R/V *Ronald H. Brown*. This work was funded by the Global Carbon Cycle project of the NOAA Office of Global Programs grants NA06GP048 (M. D. D.), NA17RJ1223 (W. R. M.), and NA87RJ0445 (W. R. M.) and by National Science Foundation grant OCE-9986724 (W. R. M.).

References

Baehr, M. M., and M. D. DeGrandpre (2004), In situ pCO_2 and O_2 measurements in a freshwater lake during turnover and stratification: Observations and a model, *Limnol. Oceanogr.*, *49*, 330–340.

Barber, R. T., and F. P. Chavez (1991), Regulation of primary productivity rate in the equatorial Pacific, *Limnol. Oceanogr.*, *36*, 1803–1815.

Bates, N. R., T. Takahashi, D. W. Chipman, and A. H. Knapp (1998), Variability of pCO_2 on diel to seasonal time scales in the Sargasso Sea, *J. Geophys. Res.*, *103*, 15,567–15,585.

Bidigare, R. R., B. B. Prézelin, and R. C. Smith (1992), Bio-optical models and the problems of scaling, in *Primary Productivity and Biogeochemical Cycles in the Sea*, edited by P. G. Falkowski and A. D. Woodhead, pp. 175–212, Plenum, New York.

Boutin, J., et al. (1999), Satellite sea surface temperature: A powerful tool for interpreting in situ pCO_2 measurements in the equatorial Pacific Ocean, *Tellus*, *Ser. B*, *51*, 490–508.

Chai, F., R. C. Dugdale, T.-H. Peng, F. P. Wilkerson, and R. T. Barber (2002), One-dimensional ecosystem model of the equatorial Pacific upwelling system: I. Model development and silicon and nitrogen cycle, *Deep Sea Res.*, *Part II*, *49*, 2713–2745.

Chavez, F. P., P. G. Strutton, G. E. Friederich, R. A. Feely, G. C. Feldman, D. G. Foley, and M. J. McPhaden (1999), Biological and chemical response of the equatorial Pacific Ocean to the 1997–1998 El Niño, *Science*, *286*, 2126–2131.

Cooper, D. J., A. J. Watson, and P. D. Nightingale (1996), Large decrease in ocean-surface CO_2 fugacity in response to in situ iron fertilization, *Nature*, *383*, 511–513.

Cosca, C. E., R. A. Feely, J. Boutin, J. Etcheto, M. J. McPhaden, F. P. Chavez, and P. G. Strutton (2003), Seasonal and interannual CO_2 fluxes for the central and eastern equatorial Pacific Ocean as determined from fCO_2-SST relationships, *J. Geophys. Res.*, *108*(C8), 3278, doi:10.1029/2000JC000677.

Cullen, J. J., M. R. Lewis, C. O. Davis, and R. T. Barber (1992), Photosynthetic characteristics and estimated growth rates indicate grazing is the proximate control of primary production in the equatorial Pacific, *J. Geophys. Res.*, *97*, 630–654.

Dandonneau, Y. (1995), Sea-surface partial pressure of carbon dioxide in the eastern equatorial Pacific (August 1991 to October 1992): A multivariate analysis of physical and biological factors, *Deep Sea Res.*, *Part II*, *42*, 349–364.

DeGrandpre, M. D., T. R. Hammar, and C. D. Wirick (1998), Short-term pCO_2 and O_2 dynamics in California coastal waters, *Deep Sea Res., Part II*, *45*, 1557–1575.

Dickson, A. G., and F. J. Millero (1987), A comparison of the equilibrium constants for the dissociation of carbonic acid in seawater media, *Deep Sea Res.*, *34*, 1733–1743.

Feely, R. A., R. Wanninkhof, H. B. Milburn, C. E. Cosca, M. Stapp, and P. P. Murphy (1998), A new automated underway system for making high precision pCO_2 measurements onboard research ships, *Anal. Chim. Acta*, *377*, 185–191.

Feely, R. A., et al. (2002), Seasonal and interannual variability of CO_2 in the equatorial Pacific, *Deep Sea Res.*, *Part II*, *49*, 2443–2469.

Gao, Y., S.-M. Fan, and J. L. Sarmiento (2003), Aeolian iron input to the ocean through precipitation scavenging: A modeling perspective and its implication for natural iron fertilization in the ocean, *J. Geophys. Res.*, *108*(D7), 4221, doi:10.1029/2002JD002420.

Inoue, H. Y., and Y. Sugimura (1992), Variations and distributions of CO_2 in and over the equatorial Pacific during the period from the 1986/88 El Niño event to the 1988/89 La Niña event, *Tellus, Ser. B*, *44*, 1–22.

Johnson, G. C., C. L. Sabine, K. E. McTaggart, and J. M. Hummon (2004), Physical oceanographic conditions during GasEx 2001, *J. Geophys. Res.*, *109*, C08S04, doi:10.1029/2002JC001718.

Johnson, K. M., A. E. King, and J. M. Seiburth (1985), Coulometric TCO_2 analyses for marine studies: An introduction, *Mar. Chem.*, *16*, 61–82.

Langdon, C. (1984), Dissolved oxygen monitoring system using a pulsed electrode: Design, performance, and evaluation, *Deep Sea Res.*, *31*, 1357–1367.

Langdon, C., J. Marra, and C. Knudson (1995), Measurements of net and gross O_2 production, dark O_2 respiration, and ^{14}C assimilation at the Marine Light-Mixed Layers site (59°N, 21°W) in the northeast Atlantic Ocean, *J. Geophys. Res.*, *100*, 6645–6653.

Laws, E. A. (1991), Photosynthetic quotients, new production and net community production in the open ocean, *Deep Sea Res.*, *38*, 143–167.

Lefèvre, N., C. Andrié, Y. Dandonneau, G. Reverdin, and M. Rodier (1994), pCO_2, chemical properties, and estimated new production in the equatorial Pacific in January–March 1991, *J. Geophys. Res.*, *99*, 12,639–12,654.

Liss, P. S., and L. Merlivat (1986), Air-sea gas exchange rates: Introduction and synthesis, in *The Role of Air-Sea Exchange in Geochemical Cycling*, *NATO ASI Ser. C, Math. Phys. Sci*., vol. 185, edited by P. Buat-Menard, pp. 113–128.

McGillis, W. R., et al. (2004), Air-sea CO_2 exchange in the equatorial Pacific, *J. Geophys. Res.*, doi:10.1029/2003JC002256, in press.

McNeil, C. L., and D. M. Farmer (1995), Observations of the influence of diel convection on upper ocean dissolved gas measurements, *J. Mar. Res.*, *53*, 151–169.

Murray, J. W., R. T. Barber, M. R. Roman, M. P. Bacon, and R. A. Feely (1994), Physical and biological controls on carbon cycling in the equatorial Pacific, *Science*, *266*, 58–65.

Platt, T., and A. D. Jassby (1976), The relationship between photosynthesis and light for natural assemblages of coastal marine phytoplankton, *J. Phycol.*, *12*, 421–430.

Platt, T., C. L. Gallegos, and W. G. Harrison (1980), Photoinhibition of photosynthesis in natural assemblages of marine phytoplankton, *J. Mar. Res.*, *38*, 687–701.

Price, J. F., R. A. Weller, and R. Pinkel (1986), Diel cycling: Observations and models of the upper ocean response to diel heating, cooling, and wind mixing, *J. Geophys. Res.*, *91*, 8411–8427.

Sabine, C. L., R. A. Feely, G. C. Johnson, P. G. Strutton, M. F. Lamb, and K. E. McTaggart (2004), A mixed layer carbon budget for the GasEx-2001 experiment, *J. Geophys. Res.*, *109*(C8), C08S05, doi:10.1029/2002JC001747.

Steinberg, P. A., F. J. Millero, and X. Zhu (1998), Carbonate system response to iron enrichment, *Mar. Chem.*, *62*, 31–43.

Strutton, P. G., F. P. Chavez, R. C. Dugdale, and V. Hogue (2004), Primary productivity in the central equatorial Pacific (3°S 130°W) during GasEx-2001, *J. Geophys. Res.*, *109*, C08S06, doi:10.1029/2003JC001790.

Takahashi, T., et al. (2002), Global sea-air CO_2 flux based on climatological surface ocean pCO_2, and seasonal biological and temperature effects, *Deep Sea Res.*, *Part II*, *49*, 1601–1622.

Van Scoy, K. A., K. P. Morris, J. E. Robertson, and A. J. Watson (1995), Thermal skin effect and the air-sea flux of carbon dioxide: A seasonal high-resolution estimate, *Global Biogeochem. Cycles*, *9*, 253–262.

Walsh, I. D., S. P. Chung, M. J. Richardson, and W. D. Gardner (1995), The diel cycle in the integrated particle load in the equatorial Pacific: A comparison with primary production, *Deep Sea Res.*, *Part II*, *42*, 465–477.

Wanninkhof, R. (1992), Relationship between wind speed and gas exchange over the ocean, *J. Geophys. Res.*, *97*, 7373–7382.

Wanninkhof, R., and K. Thoning (1993), Measurement of fugacity of CO_2 in surface water using continuous and discrete sampling methods, *Mar. Chem.*, *44*, 189–204.

Wanninkhof, R., R. A. Feely, D. K. Atwood, G. Berberian, D. Wilson, P. P. Murphy, and M. F. Lamb (1995), Seasonal and lateral variations in carbon chemistry of surface water in the eastern equatorial Pacific during 1992, *Deep Sea Res.*, *Part II*, *42*, 387–409.

Ward, B., R. Wanninkhof, W. R. McGillis, A. T. Jessup, M. D. DeGrandpre, J. E. Hare, and J. B. Edson (2004), Biases in the air-sea flux of CO_2 resulting from ocean surface temperature gradients, *J. Geophys. Res.*, *109*(C8), C08S08, doi:10.1029/2003JC001800.

Watson, A. J., C. S. Law, K. A. Van Scoy, F. J. Millero, W. Yao, G. E. Friederich, M. I. Liddicoat, R. H. Wanninkhof, R. T. Barber, and K. H. Coale (1994), Minimal effect of iron fertilization on sea-surface carbon dioxide concentrations, *Nature*, *371*, 143–145.

Weiss, R. F. (1974), Carbon dioxide in water and seawater: The solubility of a non-ideal gas, *Mar. Chem.*, *2*, 203–215.

Williams, P. J. L. B. (1998), The balance of plankton respiration and photosynthesis in the open oceans, *Nature*, *394*, 55–57.

M. D. DeGrandpre, Department of Chemistry, University of Montana, Missoula, MT 59812, USA. (michael.degrandpre@umontana.edu)

W. R. McGillis, Geochemistry, Lamont-Doherty Earth Observatory, Columbia University, Palisades, NY 10964, USA. (wrm2102@columbia.edu)

P. G. Strutton, College of Oceanic and Atmospheric Sciences, Oregon State University, Corvallis, OR 97331, USA. (strutton@coas.oregonstate.edu)

R. Wanninkhof, Atlantic Oceanographic and Meteorological Laboratory, National Oceanic and Atmospheric Administration, Miami, FL 33149, USA. (rik.wanninkhof@noaa.gov)